Ice nucleation by surrogates of Martian mineral dust: What can we learn about Mars without leaving Earth?

Citation: Cziczo, Daniel J., Sarvesh Garimella, Michael Raddatz, Kristina Hoehler, Martin Schnaiter, Harald Saathoff, Ottmar Moehler, Jonathan P. D. Abbatt, and Luis A. Ladino. "Ice Nucleation by Surrogates of Martian Mineral Dust: What Can We Learn About Mars Without Leaving Earth?" Journal of Geophysical Research: Planets 118 (September 2013): 1945-1954.

As Published: http://dx.doi.org/10.1002/jgre.20155

Publisher: American Geophysical Union

Persistent URL: http://hdl.handle.net/1721.1/87715

Version: Final published version: final published article, as it appeared in a journal, conference proceedings, or other formally published context

Ice nucleation by surrogates of Martian mineral dust: What can we learn about Mars without leaving Earth?

Daniel J. Cziczo,[1] Sarvesh Garimella,[1] Michael Raddatz,[2] Kristina Hoehler,[3] Martin Schnaiter,[3] Harald Saathoff,[3] Ottmar Moehler,[3] Jonathan P. D. Abbatt,[4] and Luis A. Ladino[4]

Received 11 June 2013; revised 30 August 2013; accepted 7 September 2013; published 23 September 2013.

[1] Water and carbon dioxide ice clouds have been observed in the Martian atmosphere where they are dynamic parts of that planet's water and carbon cycles. Many Martian atmospheric models struggle to correctly predict clouds and, with insufficient data, some use untested simplifications that cloud formation occurs exactly at the saturation point of the condensed phase or at the same conditions as terrestrial cirrus clouds. To address the lack of data, we have utilized an 84 m^3 cloud chamber built for studies of high altitude cirrus and polar stratospheric ice clouds in the Earth's atmosphere and adapted to Martian conditions. Using this chamber, we have been able to produce water ice clouds from aerosol in an inert and low pressure atmosphere mimicking that of Mars. At temperatures between 189 and 215 K, we investigated cloud formation by mineral dust particulates of a similar composition and size to those found on Mars. We show that these surrogate materials nucleate effectively at the higher temperatures, with minor temperature dependence at saturations ratios with respect to the ice phase of ~1.1, similar to what has been found for terrestrial cirrus. At the lower end of the temperature range, this saturation rises to ~1.9, a result consistent with previous studies.

Citation: Cziczo, D. J., S. Garimella, M. Raddatz, K. Hoehler, M. Schnaiter, H. Saathoff, O. Moehler, J. P. D. Abbatt, and L. A. Ladino (2013), Ice nucleation by surrogates of Martian mineral dust: What can we learn about Mars without leaving Earth?, *J. Geophys. Res. Planets*, *118*, 1945–1954, doi:10.1002/jgre.20155.

1. Introduction

[2] Martian clouds are an important part of the planet's carbon and water cycles [*Clancy et al*., 1996; *Owen*, 1992]. Unlike terrestrial clouds, those on Mars are only a single phase (ice) but can be composed of both water and carbon dioxide [*Kahn*, 1990; *Owen*, 1992; *Hu et al*., 2012]. Measurements have been made both via remote sensing (from Martian orbit or Earth) and in situ using, e.g., the Phoenix light detection and ranging (lidar) instrument [*Whiteway et al*., 2008 and *Whiteway et al*., 2009] which showed significant low level water ice clouds at 3–5 km altitude and temperatures (T) as high as ~210 K. *Whiteway et al*. (2009) also observed ice clouds as low as 1 km and temperatures as high as 218 K. In general, water ice clouds on Mars are believed to form at T between 135 and 210 K and water vapor partial pressure (P) from ~10^{-4} to 10^{-6} mbar [*Colaprete et al*., 1999; *Iraci et al*., 2010].

[3] Models from single cloud resolving to planetary scale have been developed to describe the nucleation, evolution, and precipitation of these clouds [*Pathak et al*., 2008; *Daerden et al*., 2010; *Montmessin et al*., 2002; *Montmessin et al*., 2004]. Several models consider cloud nucleation and microphysics, which have not been directly measured, by simple assumptions and/or analogies to terrestrial observations. Simple assumptions include that of *Davy et al*. [2009], who treat the nucleation of clouds at exactly the equilibrium saturation and freezing point. Terrestrial analogies of cloud formation, in the absence of Martian samples and in situ measurements, include assumption of Earth-like ice nuclei (IN) by *Michelangeli et al*. [1993]. *Määttänen et al*. [2005], using classical heterogeneous nucleation theory (CHNT) and an assumption of Earth-like particle surfaces, calculated a required, or critical, nucleation saturation ratio with respect to water ice (S_{crit}) similar to Earth conditions (of ~1.2, equivalent to 120% relative humidity with respect to ice or RH_i).

[4] The concept of using terrestrial analogs for Martian clouds focuses on comparisons to the fully glaciated (i.e., completely frozen) clouds found high in the Earth's troposphere [*Iraci et al*., 2010]. Termed cirrus, these clouds have been extensively studied in the lab and in situ due to their climatic importance [*Lynch et al*., 2002; *Cziczo et al*., 2013]. Cirrus frequently nucleate in the low T (~ 200 K) and total p (~ 100 mbar) conditions of the upper troposphere

[1]Department of Earth, Atmospheric, and Planetary Sciences, Massachusetts Institute of Technology, Cambridge, Massachusetts, USA.
[2]Department of Physics, Leibniz Institute for Tropospheric Research, Leipzig, Germany.
[3]Institute for Meteorology and Climate Research, Karlsruhe Institute of Technology, Karlsruhe, Germany.
[4]Department of Chemistry, University of Toronto, Toronto, Ontario, Canada.

Corresponding author: D. J. Cziczo, Department of Earth, Atmospheric, and Planetary Sciences, Massachusetts Institute of Technology, Cambridge, MA 02141, USA. (djcziczo@mit.edu)

2169-9097/13/10.1002/jgre.20155

[*Lynch et al*., 2002]. This represents a similar T but somewhat higher p than, but not grossly dissimilar to, the lower Martian atmosphere. Comparisons of Martian clouds to Polar Stratospheric Clouds (PSCs) are more tenuous because the ice nucleation mechanisms (described in the next paragraphs) are not the same [*Solomon*, 1999].

[5] From cirrus studies, the process of ice nucleation is known to proceed along two pathways: homogenous and heterogeneous ice nucleation. Homogeneous freezing is the process by which a water ice "embryo" spontaneously forms from within the liquid phase. There is a kinetic barrier to the formation of the ice phase and it proceeds at conditions far from equilibrium: 40 K below the bulk freezing point and at a saturation ratio (SR_i) > 1.5 [*Koop et al*., 2000]. Homogeneous freezing is the likely mechanism that leads to terrestrial PSC formation [*Solomon*, 1999]. Conversely, Määttänen et al. [*Määttänen et al*., 2005, and references therein] have shown that homogeneous freezing is unlikely at the T and p conditions found in the Martian atmosphere. The more likely cloud formation process for Mars is heterogeneous ice nucleation. Heterogeneous ice nucleation requires the presence of a preexisting particle, termed an ice nucleus (IN), which stabilizes the nascent ice embryo. There are several heterogeneous ice nucleation pathways which are important on Earth but not Mars since they proceed from an initial liquid water state. The relevant process for Mars, termed "depositional nucleation," does not require droplets. Instead, ice directly deposits from the vapor phase to the IN [*Pruppacher and Klett*, 1997; *Lynch et al*., 2002]. The most common IN in the Earth's atmosphere are mineral dust particles [*Pruppacher and Klett*, 1997; *DeMott et al*., 2003; *Cziczo et al*., 2013]. The ubiquity of dust in the Martian atmosphere [*Tomasko et al*., 1999] suggests that this is true for Mars as well. This assumption is made in most Martian cloud models [*Pathak et al*., 2008; *Montmessin et al*., 2002; *Michelangeli et al*., 1993; *Colaprete et al*., 1999]. The consequence of the assumption of mineral dust IN allows for the aforementioned choice of S_{crit}.

[6] Studies of terrestrial cirrus ice nucleation have generally followed two paths: in situ studies and laboratory experiments where cirrus formation conditions are mimicked. Field studies are less adaptable to Martian topics since, in most cases, the specific nucleation T and SR_i are not determined (i.e., the cloud has formed before sampling occurs) and the aerosol contains types only present on Earth (e.g., biomass burning and sea salt) [*Cziczo et al*., 2004]. Experimental studies using chambers in which ice crystals are nucleated on particles suspended in the gas phase are the more relevant since T, p, SR_i, and aerosol size and composition can be varied. Commonly studied mineral dusts include Arizona Test Dust (ATD) and various clays. The S_{crit} reported for ice nucleation by these mineral dusts at 210 < T < 260 K varies from ~1.1 to 1.5 with most studies showing significant ice formation (i.e., >1% of particles) at ~1.2–1.3 [*Archuleta et al*., 2005; *DeMott et al*., 2003; *Dymarska et al*., 2006; *Kanji et al*., 2008; *Knopf and Koop*, 2006; *Moehler et al*., 2006]. Different minerals exhibit a different nucleation T at a given SR_i [*Gallavardin et al*., 2008] with a general trend of lower S_{crit} with both decreasing T and larger particle surface area [*Pruppacher and Klett*, 1997; *Archuleta et al*., 2005]. Mineral dust particles of the same composition and size are observed to form ice over a wide (10's of K) T range with some fraction not causing nucleation up to the homogeneous freezing limit. This is inferred to be due to subparticle scale features, termed "active sites," which dominate nucleation and vary from particle to particle [*Marcolli et al*., 2007]. Terrestrial studies of heterogeneous nucleation have been limited to cirrus relevant T (i.e., almost exclusively T > 200 K).

[7] *Iraci et al*. [2010] and *Phebus et al*. [2011] have considered ice nucleation under lower T conditions (below 185 K), relevant for Mars, by using a small vacuum chamber within which mineral dust is placed on a Si substrate (i.e., not freely suspended in a gas). *Iraci et al*. [2010], using clay minerals, determined a rapidly increasing S_{crit} required for ice nucleation, from 1.1 to 2.5, as T was lowered from 185 to 160 K. *Phebus et al*. [2011], using the same technique, found a similar trend for a Martian soil dust simulant with S_{crit} ~ 3.8 at 155 K. *Trainer et al*. [2009], using a similar vacuum chamber technique, considered ice nucleation on the substrate itself and combined the experimental results of *Fortin et al*. [2003] and *Shilling et al*. [2006] to span a T range from 240 to ~150 K with S_{crit} in excess of 18 at the lowest T.

[8] *Ladino and Abbatt* [2013] recently addressed the limitation of the aforementioned techniques, which requires that particles be placed on a substrate, by freely suspending mineral dust aerosol in air and exposing them to low T and SR_i > 1.0 conditions within the 2 liter University of Toronto Continuous Flow Diffusion Chamber (UT-CFDC). In brief, a CFDC operates by passing particles for ~10 s between two ice-coated plates held at different temperatures. Water vapor concentration and T vary linearly between the plates but since these quantities vary exponentially with respect to each other, a supersaturation can be created [*Kanji and Abbatt*, 2009]. *Ladino and Abbatt* [2013] used two Martian surrogate materials and three terrestrial mineral dust samples to show that the S_{crit} for ice nucleation increases as T decreases. Differences between particle types were evident but the general trend was for S_{crit} ~1.3 at ~220 K increasing to ~1.8 at ~202 K. The results of *Ladino and Abbatt* [2013] are not contradictory with studies that have concentrated on terrestrial conditions due to the focus on lower temperatures for Martian clouds. As a whole, the data imply an increase in the S_{crit} of ice nucleation at lower T. This trend (S_{crit} increasing by 2.7 from 185 to 155 K), beginning just below the value commonly considered for cirrus clouds, is the opposite sign of the flat or slight decrease in S_{crit} for mineral dust from 260 to 200 K [*Moehler et al*., 2006]. Recent observations of the Martian atmosphere appear to support high supersaturations, with values of SR_i in excess of 10 reported at 40 km by *Maltagliati et al*. [2011] using the Spectroscopy for the Investigation of the Characteristics of the Atmosphere of Mars instrument onboard Mars Express. It should be noted that Maltagliati et al. showed a rapid decline in SR_i to ~1 at 20 km. The lower altitude corresponds to both a higher T and larger concentration of IN.

[9] We have conducted a set of experiments using an 84 m^3 cloud chambers built for studies of cirrus ice clouds in which we mimicked Martian conditions. We seek to bridge the gap in the aforementioned studies by considering a range from 215 to 189 K. Experiments were conducted with freely suspended particles in an inert atmosphere (N_2) with variable water vapor. Mineral dust particles of a similar composition and size to those found on Mars [*Allen et al*., 1998;

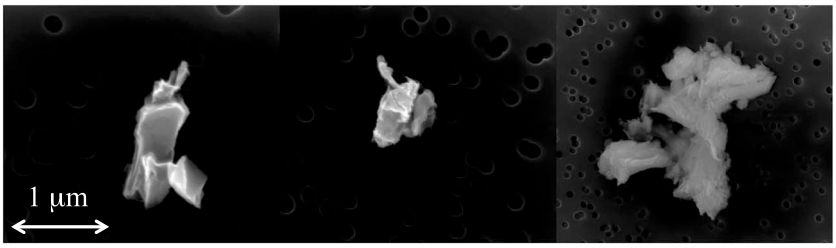

Figure 1. Environmental scanning electron microscope (ESEM) images of three individual MMS particles with common scale. These samples were collected after expansion IN-48.

Peters et al., 2008] were used as the source of IN. We observe a significant trend of increasing S_{crit} required for ice nucleation as T was lowered through this range, from ~1.1 to ~1.9. These data are interpreted in the context of fraction of aerosol nucleating ice in order to compare them to previous data sets using CHNT.

2. Experimental Methods

2.1. Mojave Mars Simulant (MMS)

[10] The particle type utilized in these studies was the MMS dust previously described by *Peters et al*. [2008]. MMS is derived from mined olivine basalt chosen due to its chemical similarity to Martian soil. Analysis by *Peters et al*. [2008] shows this material to be devoid of phyllosilicates or clay minerals, containing plagioclase feldspar and calcium rich pyroxene with minor components including magnetite, ilmenite, iron-rich olivine, and hematite. *Peters et al*. [2008] note that the mechanical generation (i.e., crushing and grinding) of this material is believed to more closely resemble processes of weathering and impact events devoid of water and organics that are common to Mars but not Earth. MMS particles were collected on electron microscope grids during the experiments described in the following sections. Three images providing typical size and surface morphology are shown in Figure 1.

2.2. Particle Generation and Size Distribution

[11] For these experiments, ground MMS was aerosolized into N_2 gas using a rotating brush disperser (RGB 1000, Palas GmbH, Karlsruhe, Germany). Multimicrometer aerosol particles were removed by passing the flow through two cyclone impactors. Prior to the experiment, the particle size distributions were analyzed using an aerodynamic particle spectrometer (APS, TSI, Inc., Shoreview, MN, USA) and two differential mobility analyzers (DMAs). A DMA can be used to select for specific particle size [see *Leinert*, 2002 and references therein] or, by scanning across particle size and when coupled to a particle counter, to determine the particle size distribution. The later configuration is commonly termed a scanning mobility particle sizer (SMPS). Differential mobility analysis functions on the principle of producing a Boltzmann distribution of charge on a particle population by passing it through a radioactive source (Po^{210} or Kr^{85}). The predominantly singly charged particles are then separated by passing them through an electrical field of known length, thereby separating them according to electrical mobility. SMPS scans across electrical mobility space result in a size distribution of the original aerosol once corrected (i.e., "inverted") for the initial charge distribution [*Leinert*, 2002]. Corrected data for MMS generated in these experiments are shown in Figure 2 from both a commercial SMPS (TSI, Inc., Shoreview, MN, USA) and the Leipzig Institute for Tropospheric Research (TROPOS) Maxi-DMA, based on the HAF-DMA (High Aerosol Flow-DMA) [*Leinert*, 2002; *Leinert and Wiedensohler*, 2008; *Raddatz et al*., 2013]. The Maxi-DMA allows for a wider size range and larger upper limit (from 0.5 to 3 micrometers diameter) than is available from commercial units. Note for comparison that Martian observations and models suggest predominantly supermicrometer mineral dust aerosol. These include *Pathak et al*. [2008]: ~1.6 μm; *Montmessin et al*. [2002]: ~1.6 μm; *Michelangeli et al*. [1993]: ~1.5 μm; *Colaprete et al*. [1999]: lognormal distribution with a mode size of 0.6 μm. A full description of mineral dust aerosol preparation and size distribution characterization is discussed by *Moehler et al*. (2006).

2.3. Aerosol Interactions and Dynamics in the Atmosphere (AIDA) Chamber

[12] Located at the Karlsruhe Institute of Technology, AIDA is an 84 m^3 aluminum chamber with a diameter of 4 m. Actively cooled, the chamber is evacuated before experiments (p <0.1 mbar) and filled with particle-free N_2. The background density of particles, determined with a Condensation Particle Counter modified to enable measurements down to p as low as 100 mbar (CPC; TSI Model 3010, Shoreview, MN, USA), was in all cases <0.1 cm^{-3}.

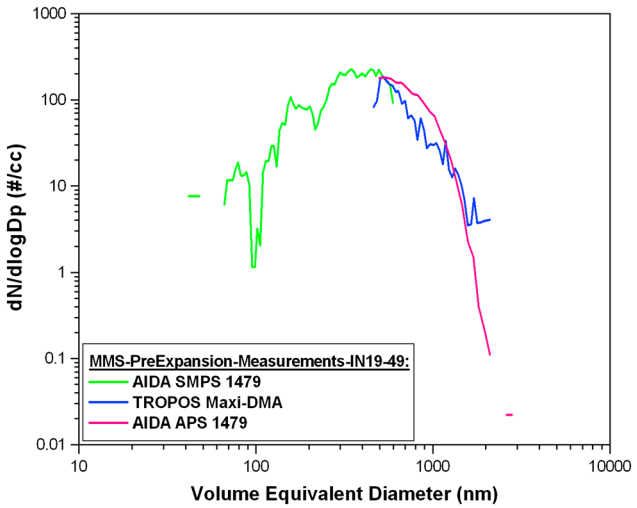

Figure 2. Size distribution, in number concentration versus size, for the MMS mineral dust particles using the AIDA SMPS, APS, and Leipzig Maxi-DMA. These data are for the aerosol in the AIDA chamber prior to expansion IN19-49.

Table 1. Experimental Parameters for AIDA Experiments

Expansion Number	Pump Speed (%)	Initial P (mbar)	Initial T (K)	SRi (1%)	T (at 1%, K)	P (at 1%, mbar)	SRi (10%)	T (at 10%, K)	P (at 10%, mbar)	Final P (mbar)	Final T (K)	Concentration (per cc)
IN19-48	80	968.3	218.2	1.09	212.2	962.2	1.12	211.7	950	798.7	208	194.8
IN19-49	80	1002.1	215.3	1.1	212.2	965.4	1.14	211.7	956	819.3	213.7	134.6
IN19-50	80	818.5	213.6	1.08	212	793.1	1.12	211.6	785.7	614.7	213.3	99
IN19-51	Reference Data	993.3	217.6	-	-	-	-	-	-	-	-	-
IN19-52	80	1000.6	213.9	1.11	211.8	962.8	1.17	211.3	951.2	799.3	207.5	133.5
IN19-53	60	992.5	217.3	1.13	212	962.9	1.19	211.3	948.6	619	213.1	88.8
IN19-54	60 - 80	1003.6	193.7	1.39	190.9	888.1	1.4	188.8	788.6	712.5	192.9	85.1
IN19-55	80	1003	194	1.91	189.2	877.7	1.94	188.2	817.8	718.3	193	52.3
IN19-56	60	1001.6	203.2	1.15	200.7	949.5	1.22	199.3	920.6	721.8	201.7	136.8

Polydisperse MMS was generated and then added to the chamber (Figure 2). For experiments described here, the chamber was initially held isothermal (±0.3°C) between 193.7 and 218.3 K (Table 1). Initial experimental p was isobaric from 818.5 to 1003.0 mbar. Chamber p was measured with an absolute capacitance manometer (MKS Type 627) with an accuracy of 0.12% of the p measurement.

[13] A partial layer of ice on the walls "set" an initial condition of $SR_i \sim 0.9$ (90% RH_i). Water vapor concentration was measured by multiple instruments including a fast scanning chilled mirror hygrometer (CMH, MBW 373LX) located outside the cooled chamber housing with the gas-phase sampled through a heated stainless steel tube. This corresponds to a measurement of total water mixing ratio (i.e., the sum of water vapor and evaporated condensed water from the aerosol and ice crystals). The hygrometer measurement is therefore considered to be gas-phase water vapor until ice nucleation and a combined measurement (i.e., upper limit of gas-phase water vapor) after ice nucleation begins. Water vapor was also measured using three tunable diode laser absorption (TDL) spectroscopy hygrometers in the near infrared at a wavelength of 1.37 μm. The hygrometers simultaneously but separately measured the concentration of water vapor and total water in the chamber with a time resolution of ~1 Hz. The difference of the two measurements is used to calculate the condensed water content. These three hygrometers are termed (1) APicT (AIDA PCI in-cloud TDL; water vapor from a multipath White cell with variable open optical path from 23 – 99 m), (2) SP-APicT (Single Path APicT; water vapor from one 4 m diameter of AIDA as the optical path), and (3) APeT (AIDA PCI extractive TDL; total water from a multipath Herriott cell with 30 m path length). The longer optical path of APicT results in this being the more sensitive instrument at the lower water vapor content at the coldest temperatures.

[14] An experiment, or "expansion," was initiated by dropping chamber p ~ 200 mbar over ~120 s using vacuum pumping. The fractional pumping speed, noted for each experiment in Table 1, provides control over the cooling rate with higher values corresponding to more rapid cooling. For the expansions described here, the cooling rates immediately prior to ice formation ranged from 0.1 to 0.3 K/s. Conditions during a typical expansion are given in the upper panel of Figure 3. The quasi-adiabatic expansion results in a drop in the gas T and a corresponding increase in SR_i. An experiment of this type is analogous to the process of uplift in an atmosphere where a rising parcel expands and cools. As SR_i increased and T decreased, ice nucleation by a fraction of the MMS particles took place. This is graphed versus expansion time in Figure 3 with the fraction f_{ice} equivalent to the number of ice crystals measured by a WELAS 2 optical particle counter [*Moehler et al*., 2008] divided by the number of aerosol particles measured by the CPC immediately prior to the expansion and accounting for the reduced pressure. This reduction is accounted for by assuming that the number of particles at time t has been reduced from the initial concentration by a factor equal to the pressure at time t divided by the initial pressure. Note that f_{ice} is defined as the first time at which a given fraction of ice has formed. Due to variability in signal, WELAS 2 may indicate multiple times at which f_{ice} has an equivalent value, including postexpansion when the ice cloud is undergoing sedimentation and evaporating. Ice nucleation continued until a combination of the sedimentation of ice depleted the gas-phase water and/or pumping was ended. At this point, the chamber relaxed back to $SR_i \sim 1.00$ with a correspondingly lower system p. A comprehensive list of the instruments used for the measurements in Figure 3 is given by *Moehler et al*. [2008] with information on the application of this technique for studies of terrestrial mineral dust ice nucleation presented by *Moehler et al*. [2006].

3. Results and Discussion

[15] Eight expansions using polydisperse MMS (Figure 2) were conducted during summer 2012 as part of the "IN19" campaign at the AIDA cloud chamber. In all cases, AIDA was filled with N_2 gas, not air, to mimic the predominantly inert Martian CO_2 atmosphere. Water vapor was then added to form the ice layer on the walls as described in the last section. Experiments were numbered IN19-48 to -56 with -51 being an instrumental reference expansion without any aerosol added to the chamber. Table 1 contains relevant experimental information. These include the initial and final p and T and the conditions (S_{crit}, T, and P) at which 1% and 10% of the MMS particles nucleated ice. Initial aerosol generation, properties, number density, and size information are also provided.

[16] Figure 3 graphically shows the effect of the expansion on the MMS particles. AIDA vacuum pumps are turned on at time = 0 with a resulting drop in p and T and increase in SR_i (upper panel). There is a small resulting decrease in particles as they sediment and/or are pumped from the system after the start of the expansion but before ice nucleates, in this case a decrease of ~10%. Just after 200 s into this expansion, IN19-55, the fraction of particles which nucleated ice and grew to a size large enough to be detected by the WELAS 2 instrument rises from 0. Thresholds fractions of 0.01 and 0.1 (i.e.,

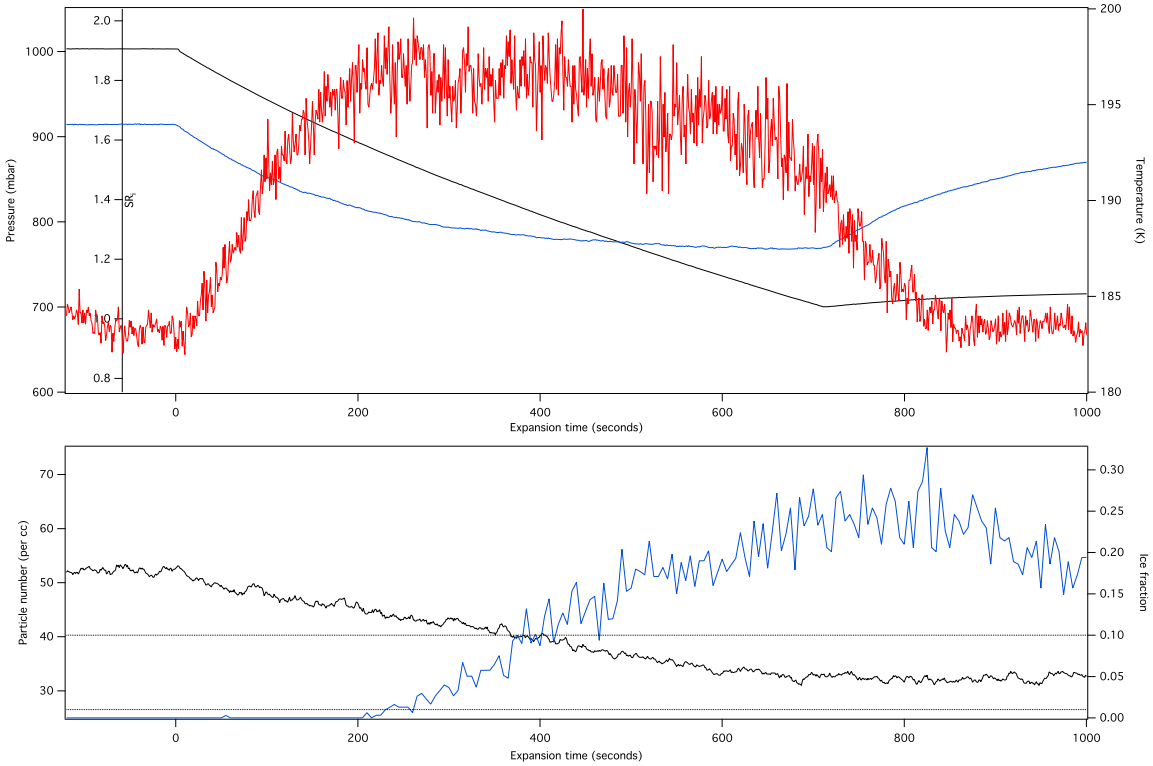

Figure 3. AIDA expansion IN19-55 (expansions 48–56 during IN19 were conducted on MMS). Top panel: gas-phase p (mbar, black trace, left axis), gas T (K, blue, right), and SRi (red, inset left) versus time (s) with 0 corresponding to the expansion start. Lower panel: concentration of particles (per cc, black trace, left axis) and fraction of particles which formed ice crystals (blue, right) as discerned by a CPC and the Welas2 instrument, respectively. Thin dotted lines indicate thresholds for 1 and 10% nucleation. The full suite of AIDA instruments is described in *Moehler et al.* [2008].

1 and 10%) are shown as the dashed lines. These fractions are surpassed at SR_i 1.91 and 1.94 at T 189.2 and 188.2, respectively, and these are termed the critical supersaturations for 1 and 10% ice nucleation (S_{crit}(1%) and (10%), respectively).

[17] SR_i continues to rise until a combination of pump shut off and/or sedimentation of ice crystals depletes the available gas-phase water vapor. In this case, SR_i levels off from ~250 to 450 s and then declines as the ice cloud in the chamber continues to sediment and eventually evaporate. At this point, the chamber equilibrates to $SR_i \sim 1.00$ at a lower system p. Two points are noteworthy: (1) two to three expansions were conducted in sequence with particle concentrations lower during subsequent expansions as particle free N_2 (but not particles) was added to increase system p and (2) AIDA was completely evacuated and refilled with both N_2 and particles before expansions IN19-48, -52, -54, and -56. The particle free gas or gas plus particle refill can be seen in the particle concentration data in Table 1.

[18] Although the longer optical path of APicT results in the more accurate water vapor measurement at these experimental conditions, only SP-APicT data were available for the last three expansions (IN19-54 to -56). The estimated error in water vapor pressure is 5% with APicT (IN19-48 to -53) and 10% with SP-APicT (IN19-54 to -56).

3.1. Ice Nucleation Fractions

[19] The fraction of particles nucleating ice shown in the lower panel of Figure 3 is the number of ice crystals detected by the WELAS 2 instrument divided by the total number of MMS particles measured by the CPC. The fraction of particles nucleating ice can be directly compared to the results of *Ladino and Abbatt* [2013], who also provide the number of ice crystals divided by the number of particles input to a CFDC as a function of supersaturation. The S_{crit}(1%) data from this study and the polydisperse data of *Ladino and Abbatt* [2013] for MMS and another Martian mineral dust surrogate (Johnson Space Center Mars-1 or JSC-1) are given as a function of T in Figure 4. We also present data for polydisperse terrestrial standard Arizona Test Dust (ATD; Powder Technology Inc., Minnesota, USA) using AIDA (S_{crit}(8%) from *Moehler et al.* [2005] and *Moehler et al.* [2006]) and from *Ladino and Abbatt* [2013] in order to extend the upper T bound from 195 to 223 K.

[20] The data exhibit a relatively constant S_{crit}, ~1.1 – 1.3, above ~215 K, consistent with previous measurements [*Archuleta et al.*, 2005; *DeMott et al.*, 2003; *Dymarska et al.*, 2006; *Kanji et al.*, 2008; *Knopf and Koop*, 2006; *Moehler et al.*, 2006]. Note that these studies all consider similar particle types, nucleating fractions, sizes, and number densities. S_{crit} is observed to increase as T decreases below ~215 K to 1.9 at 189 K. For comparison, the lowest T considered by *Ladino and Abbatt* [2013], 202 K, exhibited $S_{crit} \sim 1.75$ for MMS.

[21] *Ladino and Abbatt* [2013] present data for mineral dust aerosol produced by atomizing a water slurry and subsequent drying before input to the CFDC which we do not

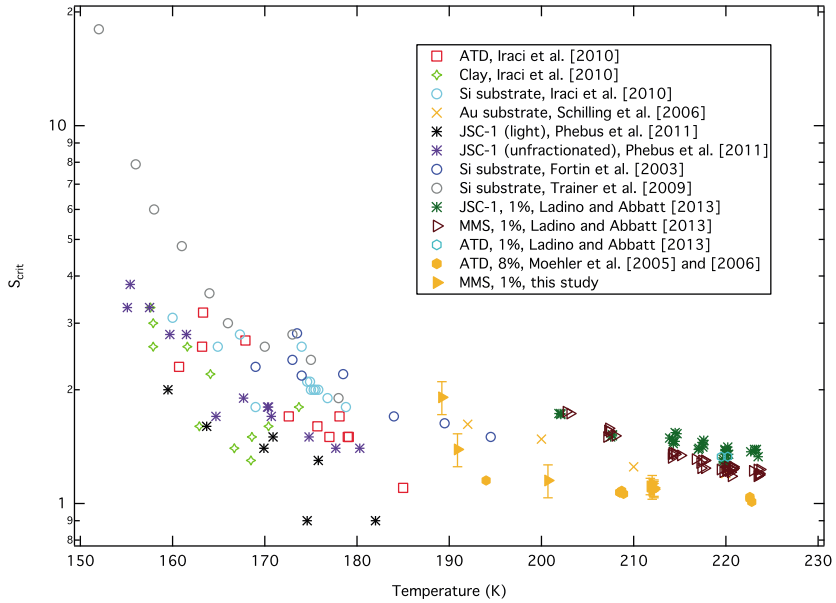

Figure 4. S_{crit} versus temperature (K) for ice nucleation from substrate-based experiments [*Fortin et al.*, 2003; Schilling et al., 2006; *Trainer et al.*, 2009; *Iraci et al.*, 2010; *Phebus et al.*, 2011], freely suspended particles in a multiliter-sized CFDC [*Ladino and Abbatt*, 2013], and the data presented here. The f_{ice} for freely suspended particle experiments is given in the caption. Error bars for these experiments are given per the information in the text. Error bars in T are in all cases smaller than the symbol size.

consider for comparison. *Ladino and Abbatt* [2013] note that for small sizes the resulting particles most likely only contain soluble material from the original sample and not mineral dust. This observation has previously been made by *Herich et al.* [2009] and helps to explain the data of *Archuleta et al.* [2005]; *Welti et al.* [2009] and *Kanji et al.* [2008]. Because of the uncertainty associated with the absence of mineral dust in some particles and the modification of surfaces due to redistribution of soluble material, we suggest that atomization of slurries not be used for freely suspended particle studies unless the samples are washed thoroughly beforehand and large enough particles are studied.

[22] The following sections include a comparison of these data with previous studies. It should be noted that there exists uncertainty in these results due to the reduced atmospheric pressure on Mars compared to our experiments and on the possibility of different nucleation kinetics. For example, Martian surface atmospheric pressure is only 0.06% of that on Earth. Large pressure differences have been shown to have an effect on nucleation of droplet formation [*Wedekind et al.*, 2008; *Hyvärinen et al.*, 2010] as well as on homogeneous freezing. [*Koop*, 2004] due to the heat transfer aspect of the atmosphere. According to *Wedekind et al.* [2008], at highly reduced overall pressure maintenance of the same amount of condensate can lead to insufficient removal of latent heat and increasingly nonisothermal effects which would reduce the nucleation rate. The pressure effect is expected to be reduced for heterogeneous nucleation due to the thermal inertia of the IN.

3.2. Heterogeneous Nucleation Theory and Comparison to Ice Nucleation Fractions

[23] A theoretical framework to describe ice nucleation by an insoluble IN, CHNT, has been summarized by *Pruppacher and Klett* [1997]. For deposition nucleation, this theory can be visualized as the formation and subsequent growth of an ice embryo, in the form of a spherical cap on the dust particle, directly from the vapor (i.e., there is no intermediate liquid water state). The particle on which the embryo forms is termed the IN to differentiate it from "interstitial" or "unactivated" particles which do not nucleate ice. CHNT assumes that nucleation is proportional to surface area and that all available surface has the same ability to nucleate ice (the "contact parameter"; see *Pruppacher and Klett* [1997] and references therein). CHNT predicts a slight increase in S_{crit} as T is lowered [*Hoose et al.*, 2010]. Larger particles are better IN than smaller ones due not only to their larger surface area but also because the saturation vapor pressure of water ice over a curved surface is greater than over a more planar one. This argument considers a perfectly spherical particle, which is not likely valid for dust particles with a high degree of surface roughness and thus a variety of different surface curvatures, even concave (Figure 1). Considering a monodisperse population of particles, CHNT predicts that all would nucleate ice at precisely the same SR_i at a given T. Considering a polydisperse population, CHNT predicts that the largest would nucleate ice at higher probability, followed by the next smaller and so on. According to the CHNT method of *Pruppacher and Klett* [1997] and *Trainer et al.* [2009], the rate of nucleation per unit surface area J (events cm^{-1} s^{-1}) on a particle's surface is:

$$J = A \exp[-\Delta F/kT] \quad (1)$$

where k is the Boltzmann constant (1.38807×10^{-16} erg K^{-1}), T is the temperature (K), and ΔF is the free energy (erg) of embryo formation on the particle surface. A is a T and S_{crit}-dependent parameter with units of cm^{-2} s^{-1}. Given by equation (9-8a) in *Pruppacher and Klett* [1997], in the cirrus regime ($T > 200$ K, $S_{crit} \sim 1.0$) J is considered

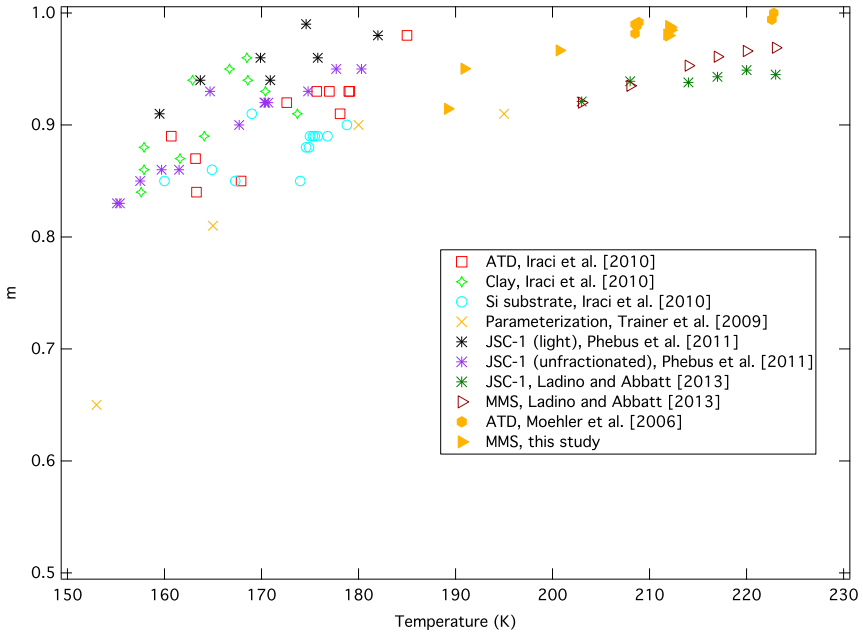

Figure 5. Contact parameter m as a function of temperature (K) for this study and the polydisperse data from *Ladino and Abbatt* [2013] calculated according to the method in section 3.2. The data are compared to the temperature-dependent parameterization of *Trainer et al*. [2009] and calculated m values from *Iraci et al*. [2010] and *Phebus et al*. [2011].

to be insensitive to A within several orders of magnitude. Values from 10^{16} of 10^{25} are suggested in the literature [*Pruppacher and Klett*, 1997; *Trainer et al*., 2009; *Ladino and Abbatt*, 2013]. *Trainer et al*. [2009] suggest that a variable A must be considered at $T < 200$ and $S_{crit} >> 1.0$:

$$A = \left(\left(\pi P_{nuc} a_g{}^2 c_i\right)/\left(2\pi m_w kT\right)^{0.5}\right) \text{ x } \left(\left(3v_i \ln S_{crit}\right)/\left(24\pi^2 a_g{}^3\right)\right)^{0.5} \quad (2)$$

where P_{nuc} is the partial pressure of water at the nucleation event (Pa), a_g is the critical size of the ice embryo (cm), c_i is the surface concentration of water monomers (1×10^{15} molecules cm^{-2}), m_w is the mass of a water molecule (2.99×10^{-23} g), and v_i is the volume of a molecule of water ice (3.22×10^{-23} cm^3 $molecule^{-1}$). The critical size of the ice embryo is also a function of S_{crit}:

$$a_g = \left(2M_w \sigma_{s/v}\right)/\left(RT\rho_{ice} \ln S_{crit}\right) \quad (3)$$

where R is the universal gas constant (8.31×10^7 erg mol^{-1} K^{-1}) and ρ_{ice} is the density of ice (9.22×10^5 g/cm^3). The surface tension at the ice/vapor interface (erg cm^{-2}) is given by *Hale and Plummer* [1974]:

$$\sigma_{s/v} = 141\text{–}0.15\ T \quad (4)$$

[24] The free energy of embryo formation is dependent on the contact parameter m. Unitless, m has a value from 1 to −1 where the former corresponds to an IN that perfectly matches the structure of ice and the later a completely dissimilar surface:

$$\Delta F = f(m,x)\left(\left(4\pi a_g{}^2 \sigma_{s/v}\right)/3\right) \quad (5)$$

where *Pruppacher and Klett* [1997] give the matching function f(m,x):

$$2f(m,x) = 1 + ((1\text{-}mx).\varphi)^3 + x^3[(2\text{-}3((x\text{-}m)/\varphi)) + ((x\text{-}m).\varphi)^3] + 3mx^2((x\text{-}m)/\varphi\text{-}1) \quad (6)$$

where

$$\varphi = \left(1\text{-}2mx + x^2\right)^{0.5} \quad (7)$$

and $x = r_n/a_g$ where r_n is the particle radius (cm). The initial step in numerically solving for m is the experimental determination of the nucleation rate. In these experiments (*Kanji and Abbatt*, 2010):

$$J = f_{ice}/(SA\ t) \quad (8)$$

where f_{ice} is experimentally determined as described at the start of this section, t is the time (s) required for nucleation, and SA is the surface area of particles. For these experiments, SA is calculated according to the method of *Moehler et al*. [2006] by fitting the concentration, median diameter, and standard deviation in Table 1 with a lognormal size distribution.

[25] This increase in S_{crit} with decreasing T can be considered for a decreasing (i.e., temperature dependent) m, a dependency that is not normally considered in CHNT. The contact parameter m has been calculated for the data presented here and using the above methodology. Planar surfaces are assumed for simplicity for polydisperse size distributions based on the data collected prior to expansions (Figure 2); for these expansions, the supermicrometer diameter particles have minimal curvature effects. We compared values of A from 10^{16} to 10^{25} and find a variation in m of less than 2%. We follow the convention of

Ladino and Abbatt [2013] and present values of 10^{16}. The MMS data from these studies, calculated per the above methodology, are shown in Figure 5 and exhibit a T dependency. Temperature-dependent contact parameters have been suggested by *Trainer et al*. [2009], *Iraci et al*. [2010], *Phebus et al*. [2011], and *Ladino and Abbatt* [2013]. The data from these references are included in Figure 5 with m values for the polydisperse data of *Ladino and Abbatt* [2013] being calculated per the above method.

3.3. Comparison to Vacuum Chamber Data

[26] The vacuum chamber data of *Iraci et al*. [2010], *Phebus et al*. [2011], and *Trainer et al*. [2009] have significant differences from this study. Vacuum chamber experiments are conducted by cooling a macroscopic substrate exposed to a fixed concentration of water vapor until ice nucleation can be detected, e.g., by Fourier Transform Infrared (FTIR) absorption. *Trainer et al*. [2009] considered ice nucleation by a Si or Au substrate while *Iraci et al*. [2010] and *Phebus et al*. [2011] reported Si substrate ice nucleation and also considered substrates coated with a dried but initially water or acetone slurry of different clays, ATD, a smectite-rich clay, and JSC-1. The advantage of vacuum chamber experiments is that lower temperatures have been possible than available to CFDCs and AIDA. An ice nucleating fraction is not determined, however, since the entire substrate is covered with mineral dust. As such, the entire surface area is considered able to nucleate ice. Ice nucleation rate is therefore related to the entire planar surface area (without the curvature effect described in the previous section) for vacuum chamber data [*Trainer et al*., 2009]. The vacuum chamber data of *Iraci et al*. [2010], *Phebus et al*. [2011], and *Trainer et al*. [2009] are plotted in Figure 4. The comparison of these to the freely suspended particle data is not straightforward since the area upon which nucleation can occur is not similar. As described by *Ladino and Abbatt* [2013], the vacuum chamber data likely correspond to an ice nucleating fraction of $<<1\%$ (i.e., the available surface area on the vacuum chamber substrate is much larger than that present in the aerosol phase in either the CFDC or AIDA experiments of Ladino and Abbatt or this work, respectively). A more relevant comparison is to the contact parameter m presented in Figure 5 which, as described in the last section, represents the relationship between the surface and the ice phase.

[27] There are noteworthy limitations to CHNT and the comparison of freely suspended particles to the substrate data. First, recent experimental studies show that even within a monodisperse sample of one particle type (e.g., mineral dust) some particles nucleate ice at higher T and/or lower SRi than others [*Marcolli et al*., 2007]. This has been interpreted as a modification to the theory presented here with different portions of a particle's surface having different contact parameters; this is not accounted for in CHNT. Second, certain particles will have a statistically favorable area with a higher contact parameter that enables ice nucleation more readily than average [*Niedermeier et al*., 2011]. This implies that a larger available surface area, such as in the vacuum chamber experiments, provides a higher probability of more active sites, such as that available in the CFDC and AIDA experiments. This is true even within CFDC and AIDA experiments where larger particles of the same composition have been observed to nucleate ice at a higher T and/or lower SR_i [*Gallavardin et al*., 2008]. Third, as noted by *Ladino and Abbatt* [2013], artifacts due to redistribution of soluble material are of concern for experiments where a slurry was used to coat a substrate as is the case in the work of *Iraci et al*. [2010] and *Phebus et al*. [2011].

4. Conclusions

[28] We have used a new method, a quasi-adiabatic expansion within an 84 m^3 chamber, to study Martian cloud formation. Ice nucleation experiments at ~215 K using mineral dust particulates of a similar composition and size to those found on Mars [*Allen et al*., 1998; *Peters et al*., 2008] show effective ice nucleation by 1% of particles at saturations ratios with respect to the ice phase of 1.1, consistent with terrestrial mineral dust nucleation at cirrus formation conditions [*Archuleta et al*., 2005; *DeMott et al*., 2003; *Dymarska et al*., 2006; *Kanji et al*., 2008; *Knopf and Koop*, 2006; *Moehler et al*., 2006]. As experimental T was reduced to 189 K, the required saturation rose to ~1.9 consistent with ice nucleation of Martian and other minerals in a vacuum chamber [*Trainer et al*., 2009; *Iraci et al*., 2010; *Phebus et al*., 2011] and freely suspended in a small cloud chamber [*Ladino and Abbatt*, 2013]. The highest saturation occurred at the higher experimental pump speed (80%) which corresponded to a higher cooling rate. Using the lower pump speed (60%) at a slightly higher T (191 K), a lower required saturation (~1.4) was observed.

[29] Furthermore:

[30] 1. The mineral dust grains did not nucleate ice at $SR_i \sim 1$, a value which has been assumed in some Martian atmospheric models [*Davy et al*., 2009]. $S_{crit} \sim 1.1$ at 215 K determined here supports the assumption of Earth-like IN by *Michelangeli et al*. [1993] and the nucleation supersaturation of ~1.2 of *Määttänen et al*. [2005] at this T. These data are consistent with previous studies of terrestrial dust [*Moehler et al*., 2006; *Cziczo et al*., 2009].

[31] 2. The substrate-based data of *Iraci et al*. [2010], *Phebus et al*. [2011], and *Trainer et al*. [2009], the latter using previous measurements of *Fortin et al*. [2003] and *Shilling et al*. [2006], are supported by freely suspended particles in the 2 liter CFDC measurements of *Ladino and Abbatt* [2013] and our data from an 84 m^3 cloud chamber. As a whole, these experiments show an increase in SR_i required for ice nucleation from ~1.1 as T is lowered from 215 K to ~4 at 160 ± 5K. We suggest that Martian cloud models use SR_i of ice nucleation as a function of T, as opposed to a fixed value. When considering CHNT, a temperature-dependent contact parameter can be used to predict this effect.

[32] Terrestrial cirrus cloud chambers provide a readily available set of state-of-the-art instrumentation which can be leveraged to the topic of Martian clouds. These chambers come with experimental limits which normally extended to the observed formation conditions of cirrus (e.g., ~200 K and terrestrial P). In practice, these limits are related to system cooling capability and leak rate, respectively. These are not theoretical, but rather experimental apparatus limits so that minimal redesigns should allow for future studies at lower T and p such that the formation of CO_2 ice clouds could be considered.

[33] **Acknowledgments.** The authors would like to thank A. Bauer, O. Stetzer, R. Hu, K. Cahoy, and M. Zuber for useful discussions. We also thank Luther Beegle (JPL) for providing the MMS sample and Nadine Hoffmann and Alexei Kiselev (KIT) for providing the ESEM measurements shown in Figure 1. We are grateful for the logistical and technical support provided by the AIDA staff. Funding was provided by the MIT International Science and Technology Initiative-Germany (MISTI-Germany), and the European project EUROCHAMP2 (Transnational Access Activity E2-2012-05-14-0075). The AIDA work was partly funded by the DFG HALO priority program SPP 1294 (contract number MOEH 668/1-2).

References

Allen, C. C., K. M. Jager, R. V. Morris, D. J. Lindstrom, M. M. Lindstrom, and J. P. Lockwood (1998), Martian soil simulant available for scientific, educational study, *Eos Trans. AGU*, *79*, 405–409.

Archuleta, C., P. DeMott, and S. Kreidenweis (2005), Ice nucleation by surrogates for atmospheric mineral dust and mineral dust/sulfate particles at cirrus temperatures, *Atmos. Chem. Phys.*, *5*, 2617–2634.

Clancy, R. T., A. W. Grossman, M. J. Wolff, P. B. James, D. J. Rudy, Y. N. Billawala, B. J. Sandor, S. W. Lee, and D. O. Muhleman (1996), Water vapor saturation at low altitudes around Mars aphelion: A key to Mars climate?, *Icarus*, *122*, 36–62.

Colaprete, A., O. B. Toon, and J. A. Magalhães (1999), Cloud formation under Mars Pathfinder conditions, *J. Geophys. Res.*, *104*, 9043–9053.

Cziczo, D. J., P. K. Hudson, D. M. Murphy, and D. S. Thomson (2004), Single particle measurements of the chemical composition of cirrus ice residue during CRYSTAL-FACE, *J. Geophys. Res.*, *109*, D04201, doi:10.1029/2003JD004032.

Cziczo, D. J., K. D. Froyd, S. J. Gallavardin, O. Moehler, S. Benz, H. Saathoff, and D. M. Murphy (2009), Deactivation of ice nuclei due to atmospherically relevant surface coatings, *Environ. Res. Lett.*, *4*, 044013.

Cziczo, D. J., K. D. Froyd, C. Hoose, E. J. Jensen, M. Diao, M. A. Zondlo, J. B. Smith, C. H. Twohy, and D. M. Murphy (2013), Clarifying the dominant sources and mechanisms of cirrus cloud formation, *Science*, *340*, 1320–1324, doi:10.1126/science.1234145.

Daerden F., J. A. Whiteway, R. Davy, C. Verhoeven, L. Komguem, C. Dickinson, P. A. Taylor, and N. Larsen (2010), Simulating observed boundary layer clouds on Mars, *Geophys. Res. Lett.*, *37*, L04203, doi:10.1029/2009GL041523.

Davy, R., P. A. Taylor, W. Weng, and P.-Y. Li (2009), A model of dust in the Martian lower atmosphere, *J. Geophys. Res.*, *114*, D04108, doi:10.1029/2008JD010481.

DeMott, P. J., D. J. Cziczo, A. Prenni, D. M. Murphy, S. Kreidenweis, D. S. Thomson, and R. Borys (2003), Compositions and concentrations of atmospheric ice nuclei, *Proc. Natl. Acad. Sci. U. S. A.*, *100*, 14,655–14,660.

Dymarska, M., B. J. Murray, L. Sun, M. L. Eastwood, D. A. Knopf, and A. K. Bertram (2006), Deposition ice nucleation on soot at temperatures relevant for the lower troposphere, *J. Geophys. Res.*, *111*, D04204, doi:10.1029/2005JD006627.

Fortin, T., K. Drdla, L. Iraci, and M. Tolbert (2003), Ice condensation on sulfuric acid tetrahydrate: Implications for polar stratospheric ice clouds, *Atmos. Chem. Phys.*, *3*, 987–997.

Gallavardin, S., et al. (2008), Single particle laser mass spectrometry applied to differential ice nucleation experiments at the AIDA chamber, *Aerosol Sci. Technol.*, *42*, 773–791.

Hale, B. N., and P. L. Plummer (1974), Molecular model for ice clusters in a supersaturated vapor, *J. Chem. Phys.*, *61*, 4012.

Herich, H., T. Tritscher, A. Wiacek, M. Gysel, E. Weingartner, U. Lohmann, U. Baltensperger, and D. J. Cziczo (2009), Water uptake of clay and desert dust aerosol particles at sub- and supersaturated water vapor conditions, *Phys. Chem. Chem. Phys.*, *11*, 7804–7809.

Hoose, C., J. Kristjanssona, J.-P. Chen, and A. Hazran (2010), Classical-theory-based parameterization of heterogeneous ice nucleation by mineral dust, soot, and biological particles in a global climate model, *J. Atmos. Sci.*, *67*, 2483–2503.

Hu, R., K. Cahoy, and K. Zuber (2012), Mars Atmospheric CO_2 condensation above the North and South Poles as revealed by radio occultation, climate sounder, and laser ranging observations, *J. Geophys. Res.*, *117*, E07002, doi:10.1029/2012JE004087.

Hyvärinen, A.-P., D. Brus, J. Wedekind, and H. Lihavainen (2010), How ambient pressure influences water droplet nucleation at tropospheric conditions, *Geophys. Res. Lett.*, *37*, L21802, doi:10.1029/2010GL045013.

Iraci, L. T., B. D. Phebus, B. M. Stone, and A. Colaprete (2010), Water ice cloud formation on Mars is more difficult than presumed: Laboratory studies of ice nucleation on surrogate materials, *Icarus*, *210*, 985–991.

Kahn, R. A. (1990), Ice haze, snow, and the Mars water cycle, *J. Geophys. Res.*, *95*, 14,677–14,693.

Kanji, Z. A., and J. P. D. Abbatt (2009), The University of Toronto Continuous Flow Diffusion Chamber (UT-CFDC): A simple design for ice nucleation studies, *Aerosol Sci. Technol.*, *43*, 730–738.

Kanji, Z. A., and J. P. D. Abbatt (2010), Ice nucleation onto Arizona test dust at cirrus temperatures: effect of temperature and aerosol size on onset relative humidity, *J. Phys. Chem. A*, *114*, 935–941.

Kanji, Z. A., O. Florea, and J. P. D. Abbatt (2008), Ice formation via deposition nucleation on mineral dust and organics: dependence of onset relative humidity on total particulate surface area, *Environ. Res. Lett.*, *3*, 025004.

Knopf, D. A., and T. Koop (2006), Heterogeneous nucleation of ice on surrogates of mineral dust, *J. Geophys. Res.*, *111*, D12201, doi:10.1029/2005JD006894.

Koop, T. (2004), Homogeneous ice nucleation in water and aqueous solutions, *Z. Phys. Chem.*, *218*, 1231–1258.

Koop, T., L. Beiping, T. Athanasios, and P. Thomas (2000), Water activity as the determinant for homogeneous ice nucleation in aqueous solutions, *Nature*, *406*, 611–614.

Ladino, L. A., and J. P. D. Abbatt (2013), Laboratory investigation of Martian water ice cloud formation using dust aerosol simulants, *J. Geophys. Res. Planets*, *118*, 14–25, doi:10.1029/2012JE004238.

Leinert, S. (2002), Hygroscopicity of micrometer-sized aerosol particles: A new measurement technique, PhD thesis, University of Leipzig.

Leinert, S., and A. Wiedensohler (2008), A DMA and APS based technique for measuring aerodynamic hygroscopic growth factors of micrometer-size aerosol particles, *J. Aerosol Sci.*, *39*, 393–402.

Lynch, D. K., K. Sassen, D. Starr, and G. Stephens (Eds) (2002), *Cirrus*, Oxford Univ. Press, Oxford, UK.

Määttänen, A., H. Vehkamäki, A. Lauri, S. Merikallio, J. Kauhanen, H. Savijärvi, and M. Kulmala (2005), Nucleation studies in the Martian atmosphere, *J. Geophys. Res.*, *110*, E02002, doi:10.1029/2004JE002308.

Maltagliati, L., F. Montmessin, A. Fedorova, O. Korablev, F. Forget, and J.-L. Bertaux (2011), Evidence of water vapor in excess of saturation in the atmosphere of Mars, *Science*, *333*, 1868–1871.

Marcolli, C., T. Peter, S. Gedamke, and B. Zobrist (2007), Efficiency of immersion mode ice nucleation on surrogates of mineral dust, *Atmos. Chem. Phys.*, *7*, 5081–5091.

Michelangeli, D. V., O. B. Toon, R. M. Haberle, and J. B. Pollack (1993), Numerical simulations of the formation and evolution of water ice clouds in the Martian atmosphere, *Icarus*, *102*, 261–285.

Moehler, O., C. Linke, H. Saathoff, M. Schnaiter, R. Wagner, A. Mangold, M. Krämer, and U. Schurath (2005), Ice nucleation on flame soot aerosol of different organic carbon content, *Meteorol. Z.*, *14*, 477–484.

Moehler, O., et al. (2006), Efficiency of the deposition mode ice nucleation on mineral dust particles, *Atmos. Chem. Phys.*, *6*, 3007–3021.

Moehler, O., S. Benz, H. Saathoff, M. Schnaiter, R. Wagner, J. Schneider, S. Walter, V. Ebert, and S. Wagner (2008), The effect of organic coating on the heterogeneous ice nucleation efficiency of mineral dust aerosols, *Environ. Res. Lett.*, *3*, 025007.

Montmessin, F., P. Rannou, and M. Cabane (2002), New insights into Martian dust distribution and water-ice cloud microphysics, *J. Geophys. Res.*, *107*(E6), 5037, doi:10.1029/2001JE001520.

Montmessin, F., F. Forget, P. Rannou, M. Cabane, and R. M. Haberle (2004), Origin and role of water ice clouds in the Martian water cycle as inferred from a general circulation model, *J. Geophys. Res.*, *109*, E10004, doi:10.1029/2004JE002284.

Niedermeier, D., R. A. Shaw, S. Hartmann, H. Wex, T. Clauss, J. Voigtlander, and F. Stratmann (2011), Heterogeneous ice nucleation: exploring the transition from stochastic to singular freezing behavior, *Atmos. Chem. Phys.*, *11*, 8767–8775.

Owen, T. (1992), The composition and early history of the atmosphere of Mars, in *Mars*, edited by H. H. Kieffer et al., Univ. of Ariz. Press, Tucson, USA.

Pathak, J., D. V. Michelangeli, L. Komguem, J. Whiteway, and L. K. Tamppari (2008), Simulating Martian boundary layer water ice clouds and the lidar measurements for the Phoenix mission, *J. Geophys. Res.*, *113*, E00A05, doi:10.1029/2007JE002967.

Peters, G. H., W. Abbey, G. H. Bearman, G. S. Mungas, J. A. Smith, R. C. Anderson, S. Douglas, and L. W. Beegle (2008), Mojave Mars simulant—Characterization of a new geologic Mars analog, *Icarus*, *197*, 470–479.

Phebus, B. D., A. V. Johnson, B. Mar, B. M. Stone, A. Colaprete, and L. T. Iraci (2011), Water ice nucleation characteristics of JSC Mars-1 regolith simulant under simulated Martian atmospheric conditions, *J. Geophys. Res.*, *116*, E04009, doi:10.1029/2010JE003699.

Pruppacher, H. R., and J. D. Klett (1997), *Microphysics of Clouds and Precipitation*, 2nd ed., Kluwer, Dordrecht, Netherlands.

Raddatz, M., A. Wiedensohler, H. Wex, and F. Stratmann (2013), Size selection of sub- and super-micron clay mineral kaolinite particles using a custom-built Maxi-DMA, *AIP Conf. Proc.*, *1527*, 457–460.

Shilling, J., T. Fortin, and M. Tolbert (2006), Depositional ice nucleation on crystalline organic and inorganic solids, *J. Geophys. Res.*, *111*, D12204, doi:10.1029/2005JD006664.

Solomon, S. (1999), Stratospheric ozone depletion: A review of concepts and history, *Rev. Geophys.*, *37*, 275–316.

Tomasko, M. G., L. R. Doose, M. Lemmon, P. H. Smith, and E. Wegryn (1999), Properties of dust in the Martian atmosphere from the imager on Mars Pathfinder, *J. Geophys. Res.*, *104*, 8987–9007.

Trainer, M. G., O. B. Toon, and M. A. Tolbert (2009), Measurements of depositional ice nucleation on insoluble substrates at low temperatures: Implications for Earth and Mars, *J. Phys. Chem. C*, *113*, 2036–2040.

Wedekind, J., A.-P. Hyvärinen, D. Brus, and D. Reguera (2008), Unraveling the Pressure Effect in Nucleation, *Phys. Rev. Lett.*, *101*, 125703.

Welti, A., F. Luond, O. Stetzer, and U. Lohmann (2009), Influence of particle size on the ice nucleating ability of mineral dusts, *Atmos. Chem. Phys.*, *9*, 6705–6715.

Whiteway, J., M. Daly, A. Carswell, T. Duck, C. Dickinson, L. Komguem, and C. Cook (2008), Lidar on the Phoenix mission to Mars, *J. Geophys. Res.*, *113*, E00A08, doi:10.1029/2007JE003002.

Whiteway, J., et al. (2009), Mars water ice clouds and precipitation, *Science*, *325*, 68–70.